Inorganic Chemistry

Article

pubs.acs.org/IC

Modes of Activation of Organometallic Iridium Complexes for Catalytic Water and C−H Oxidation

Andrew J. Ingram,[†] Arron B. Wolk,[‡] Cornelia Flender,[†] Jialing Zhang,[†,§] Christopher J. Johnson,[‡] Ulrich Hintermair,[‡,∥] Robert H. Crabtree,[‡] Mark A. Johnson,*[,‡] and Richard N. Zare*[,†]

[†]Department of Chemistry, Stanford University, Stanford, California 94305-5080, United States

[‡]Department of Chemistry, Yale University, New Haven, Connecticut 06520-8107, United States

[§]Department of Chemistry, Peking University, Beijing 100871, P.R. China

[∥]Centre for Sustainable Chemical Technologies, University of Bath, Bath BA2 7AY, U.K.

Supporting Information

ABSTRACT: Sodium periodate ($NaIO_4$) is added to Cp^*Ir^{III} ($Cp^* = C_5Me_5^-$) or $(cod)Ir^I$ (cod = cyclooctadiene) complexes, which are water and C−H oxidation catalyst precursors, and the resulting aqueous reaction is investigated from milliseconds to seconds using desorption electrospray ionization, electrosonic spray ionization, and cryogenic ion vibrational predissociation spectroscopy. Extensive oxidation of the Cp* ligand is observed, likely beginning with electrophilic C−H hydroxylation of a Cp* methyl group followed by nonselective pathways of further oxidative degradation. Evidence is presented that the supporting chelate ligand in Cp*Ir(chelate) precursors influences the course of oxidation and is neither eliminated from the coordination sphere nor oxidatively transformed. Isomeric products of initial Cp* oxidation are identified and structurally characterized by vibrational spectroscopy in conjunction with density functional theory (DFT) modeling. Less extensive but more rapid oxidation of the cod ligand is also observed in the $(cod)Ir^I$ complexes. The observations are consistent with the proposed role of Cp* and cod as sacrificial placeholder ligands that are oxidatively removed from the precursor complexes under catalytic conditions.

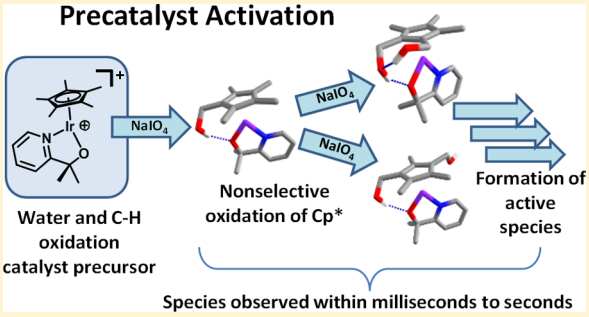

INTRODUCTION

Characterization of intermediates in molecularly defined solution-phase catalysis is a recognized means to advance rational design of catalytic performance in terms of activity, selectivity, and robustness. However, for fast reactions (i.e., $t_{1/2}$ < 1 s) this task is challenging as short-lived intermediates can be difficult to intercept and characterize by standard techniques (NMR, UV−vis, IR/Raman, etc.). Electrospray ionization (ESI) mass spectrometry (MS) and related methods are an extremely sensitive and selective means to study such reactions and characterize intermediates.[1−5] The soft ionization of electrospray methods coupled with the unique power of mass spectrometry to separate complex mixtures into their components by mass-to-charge ratio (m/z) is a powerful tool for characterizing solution species in real time that would otherwise be difficult to analyze.

Electrospray data allows us to follow catalyst speciation over time.[2,6−8] Reactive desorption electrospray ionization mass spectrometry (DESI), an ambient ionization method similar to ESI,[9−12] offers a means to initiate and sample reactions within milliseconds.[13−15] This technique has been used by the Zare lab at Stanford to characterize catalyst activation[13] and short-lived intermediates that are unstable under conventional methods and conditions.[15] To access longer time scales with ESI-MS on the order of seconds, it is possible to construct online microreactors which initiate reactions inside the tubing that leads to the electrospray source.[6] Electrosonic spray ionization (ESSI) is a variant of ESI that can use the same source as DESI to generate a spray of microdroplets.[16] In ESSI, very high flow rates of nebulizing gas generate smaller microdroplets than in ESI; these enhance solvent evaporation and can promote more efficient analyte ionization without application of an electric potential.[16,17] Furthermore, the simple and custom nature of the dual DESI/ESSI source allows for rapid cleaning/troubleshooting between experiments and increases efficiency and throughput. While exact mass and molecular formulas are readily obtained from conventional MS data, structural information is absent and isomerism is unresolved. Cryogenic ion vibrational predissociation (CIVP) spectroscopy is capable of obtaining vibrational and UV/vis spectra of mass-selected ions, allowing for structural and electronic characterization of detected species.[18,19]

Recent efforts in the Crabtree and Brudvig laboratories at Yale have produced a family of organometallic Cp*Iridium(III) complexes (Cp* = pentamethylcyclopentadienyl, $C_5Me_5^-$) as

Received: September 20, 2013
Published: November 14, 2013

   dx.doi.org/10.1021/ic402390t | Inorg. Chem. 2014, 53, 423−433

versatile precursors for highly efficient water[20] and C−H oxidation catalysis[21] with either ceric ammonium nitrate or, more recently, sodium periodate as terminal oxidants.[22,23] Subsequently, evidence was reported for oxy-functionalization of the Cp* ligand under reaction conditions, which raised questions about the molecularity and mode of action of these catalysts.[24,25] However, it was shown that when an oxidatively resistant chelate ligand is bound to the Cp*Ir fragment, total degradation of the precursors to heterogeneous iridium-oxide material is prevented.[26] Very recently, a detailed kinetic and spectroscopic study confirmed that, for a series of homogeneous oxidation catalysts, the Cp* ligand is oxidatively removed in a precatalytic activation step and that alternative sacrificial placeholder ligands, such as cod (1,5-cyclooctadiene), can be used in place of Cp* (Figure 1).[27] A bis-ligated Ir μ-oxo dimer

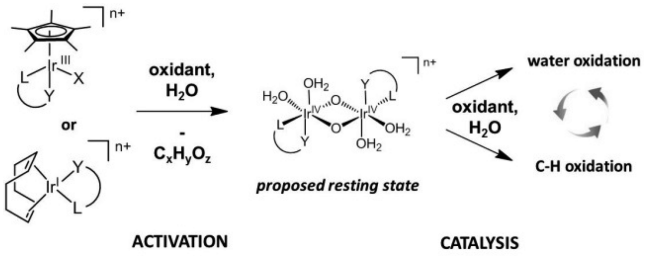

Figure 1. Proposed mode of action[27] for molecular Ir oxidation catalysts.

was proposed from ^{17}O NMR spectroscopy, resonance-Raman spectroscopy, and other data as the resting state of the catalytic species after loss of the oxidatively susceptible Cp* or cod ligands (Figure 1). The mode of oxidative precursor activation has not yet been elucidated, however, leaving significant questions regarding the importance and role of the supporting oxidatively resistant ligands in the activation process.

In this work, we present ESSI, DESI, and CIVP characterization of the oxidative activation of some Ir catalyst precursors (Scheme 1). Data obtained after time lapses from milliseconds

Scheme 1. Complexes Studied by Mass Spectrometry

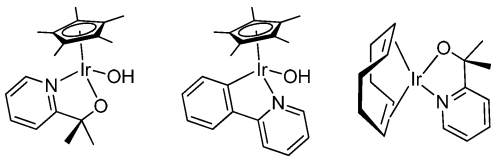

to seconds after the introduction of a chemical oxidant reveal species involved in the initial activation mechanism. We track the complex speciation using the high resolving power of an orbitrap mass analyzer.[28] As the site of initial precursor oxidation is crucial in identifying likely pathways for oxidative breakdown, a battery of isotope labeling and MS/MS fragmentation studies were performed to characterize the observed species. To obtain structural data and characterize the functional groups present in the partially oxidized precursors, we performed CIVP spectroscopy of the mass-selected ions. The vibrational spectra obtained are analogous to those found in FTIR and afforded additional structural information about these partially activated intermediates including the distinction between different isomers by infrared double resonance.

METHODS

See the Supporting Information for synthetic details.

DESI and ESSI studies were performed on a hybrid LTQ-Orbitrap-XL (ThermoFisher Scientific, San Jose, CA) with the resolution set to 100,000 at m/z 400. The custom-DESI source used has been described previously.[13,14] Briefly, it is constructed from a 1/8" stainless steel Swagelok Tee. Spray solution is pumped from a syringe and through a fused silica capillary (100 μm ID, 360 μm OD) that passes into the top of the tee and is held at its entrance point with a carefully tightened graphite ferrule. At the silica tubing's exit from the tee, the capillary runs coaxially through a 1/8" stainless steel tube. High-pressure nebulizing gas (~120 psi) is supplied through a 1/8" stainless steel tube at the bottom of the tee. The DESI source was positioned at an angle of approximately 60° from the surface, about 2 mm above the surface, and 2−4 mm from the inlet of the mass spectrometer. The ESSI studies used the same custom source as the DESI studies or a modified ESI source from a Finnigan LCQ ion trap (ThermoFisher Scientific, San Jose, CA), where the N_2 was supplied directly. The source was pointed directly at the inlet of the instrument and held approximately 4 cm away. When a source potential was required, a 0−5 kV potential was applied to the needle of the syringe supplying solution to the DESI/ESSI source. Instrument settings were as follows to ensure efficient ionization/transmission without causing significant fragmentation: capillary temperature = 175 °C, capillary voltage = 44 V, and tube lens = 110 V. Increasing the capillary voltage or tube lens above these values induced partial fragmentation of the Ir species observed and greatly complicated the interpretation of these spectra.

To acquire DESI spectra, analytes were embedded in surfaces by pipetting a small volume of a stock solution onto a surface and allowing the liquid to evaporate under a stream of N_2. Once dry, surfaces were placed underneath the DESI spray and then either rastered in front of the source or held in place until the surface was depleted of sample. The distribution of observed species varied slightly as the surface was depleted of analyte, indicating that reactions were likely occurring both in the droplets as well as on the surface, or that the observed relative distribution is highly dependent on the instantaneous concentration of analyte on the wetted surface. It is not within the scope of this study to determine whether one or both of these phenomena are occurring. Paper, glass, and porous polytetrafluoroethylene (PTFE) surfaces were tested for each compound measured. Spectra were qualitatively the same or similar for each surface type, other than an approximate order of magnitude increase in sensitivity in PTFE relative to paper and an approximately order of magnitude decrease in sensitivity in glass relative to paper. For reasons of cost and ease of handling, paper was used for most measurements unless the sensitivity of PTFE was required. The paper used was cut from manila envelopes. As DESI is an ambient ionization technique, samples are necessarily exposed to atmosphere during handling and the DESI process. When relatively air-free conditions were required, compounds were weighed in uncapped vials in a glovebox and then sealed with a septum cap. Solvents were degassed by bubbling with N_2 or Ar. Using Schlenk techniques, compounds were dissolved in degassed solvents and then syringes were used to deposit solutions on PTFE or paper surfaces which were then dried under a current of N_2 and then analyzed under air. The cod complexes are not stable in air-saturated solutions; however, when degassed dichloromethane (DCM) was used to deposit them on surfaces the solvent evaporated quickly such that extensive aerobic oxygenation of these precursors was avoided. These dry surfaces gave consistent DESI-MS when exposed to air for at least minutes.

The design for the online reactor was inspired by one in the literature,[29] where solutions of each reagent are pumped from separate syringes, through fused silica capillary tubing, and into a micromixing tee (IDEX Health and Science, Oak Harbor, WA) which effectively mixes the two solutions as they flow into the final piece of tubing which serves as a flow microreactor placed between the mixing tee and the ESSI source. Reaction times were controlled by altering residence times with different lengths of this tubing and the total flow rate. The speciation observed was indistinguishable when micromixing T's with

dx.doi.org/10.1021/ic402390t | Inorg. Chem. 2014, 53, 423−433

different dead-volumes and frit sizes were interchanged. This observation indicated that reactions did not significantly progress while the solution was in the mixing T and that the residence time in tubing is a reliable estimate of reaction time. When a source potential was required, a 0−5 kV potential was applied to the needle of the syringe supplying $NaIO_{4(aq)}$ solution to the mixing tee.

Data were analyzed using the Qualbrowser tool in ThermoScientific's Xcalibur program. When possible, m/z values were internally referenced to the m/z of $[Cp^*Ir(pyalc)]^+$, $[\mathbf{1}]^+$ (pyalc = 2-(2′-pyridyl)-2-propanolate, m/z 464.1560). Assignments of molecular formula were made by comparing the observed exact masses (within 5 ppm) as well as isotope distributions with simulated spectra. Ir-containing peaks were readily identified by the characteristic isotopic profile of Ir (^{191}Ir: 37%, ^{193}Ir: 63%; all m/z values reported here are for ^{193}Ir species), which also allowed for easy determinations of the number of Ir atoms within a given molecular formula. Because of the complexity of the spectra and the number of overlapping peaks, positive identifications were made when at least the two principal ^{191}Ir and ^{193}Ir peaks were well resolved, the exact masses were within 5 ppm, and the relative intensities were within 15%. Working with chloride-free hydroxo precursors simplified the MS spectra further by eliminating additional isotope pattern splittings. All of the detected Ir species were monocationic and monomeric, with the exception of variable and minor amounts of $[(\mathbf{Cp^*Ir})_2(\mathbf{OH})_2(\mathbf{H_2O})_n]^+$ (n = 0,1) dimers in the spectra of **1(OH)**. These were attributed to impurities in the samples of **1**, which was synthesized from $[(Cp^*Ir)_2(OH)_3]OH$. Identified Ir species in Supporting Information, Tables S1 and S2 were extracted from the MS data by exporting observed and simulated spectra as .csv files and then processing them with a custom MatLab program which identifies local maxima in the observed and simulated data and then matches peaks in the simulated spectra to peaks in the observed that are within 5 ppm. Peak areas were determined from the fit of the observed peaks to Gaussian shapes.

The Yale Cryogenic Photofragmentation Spectrometer has been described in detail elsewhere.[30,31] Briefly, electrosprayed ions were guided in RF-only multipoles through three vacuum stages to a main chamber pressure of 10^{-7} Torr. The ions were then trapped in a cryogenically cooled quadrupole ion trap (Jordan TOF Products trap mounted on a Sumitomo 4K closed-cycle cryostat) using a pulsed buffer gas mixture of 1% N_2 in He. The ions were held for 95 ms to allow for the condensation of weakly bound N_2 mass tags and the buffer gas to be evacuated before extraction into a Wiley−McLaren TOF mass spectrometer. The ions were then temporally focused and intersected with the output of an OPO/OPA infrared laser (Laservision, Belleview, WA). The tagged parent ions and photofragments formed by photoevaporation of the tag were then separated using a reflectron mass selector before detection with microchannel plates. Spectra are reported as the photofragment yield as a function of laser wavelength.

The laser fluence was lowered until a linear photofragmentation yield response was observed for all resonances. This ensures single-photon absorption, and generates spectra equivalent to linear absorption spectra, and as such can be directly compared to harmonic predictions. The OPO/OPA laser scheme is tunable from 2200 to 4500 cm^{-1} at a resolution of approximately 3 cm^{-1}. The 600−2200 cm^{-1} range was generated by mixing the signal and idler outputs in a $AgGaSe_2$ crystal, which doubles the bandwidth to around 6 cm^{-1}.

Isomer-selective CIVP spectra could be obtained using an infrared photochemical hole-burning scheme. This was achieved using infrared double resonance in conjunction with multiple stages of mass selection (IR^2MS^3) and has been described in depth in previous work.[32,33] Briefly, a second stage of mass selection was added before the reflectron to separate parent and daughters generated with the first (pump or hole-burning) laser. The undissociated parents were then interrogated at a second transient focus provided by the second (collinear) time-of-flight separator. This arrangement allowed a single isomer to be monitored at the second laser crossing while the hole-burning laser was scanned through the spectrum at the first crossing. All lines arising from the probed isomer then appeared as "dips" in the probe signal.

For all cryogenic ion vibrational predissociation experiments, an aqueous 100 μM solution of the complex was prepared with 0.4 equiv of $NaIO_4$ and allowed to equilibrate for 24 h. These solutions remained yellow in color, but exhibited large abundances of oxidized species without a high concentration of oxidant, thus avoiding salt suppression of the electrospray process. This solution was electrosprayed from a 15 μm ground silicon tip (New Objective, Woburn, MA) held at +2500 V with respect to the entrance aperture of the mass spectrometer.

Density functional calculations were carried out using the Gaussian 09 program[34] at the cam-B3LYP/SDD/6-311+G(d,p) level of theory.[35,36] Harmonic spectra were empirically scaled by 0.943 above 2500 cm^{-1} to match the calculated free OH transitions to the free OH transition in the observed $[1O]^+\cdot N_2$ spectrum. Below 2500 cm^{-1}, a scaling factor of 0.954 was applied to match the harmonic pyridine ring mode at 1613 cm^{-1}. Isomer searches were performed by sampling a grid generated by rotation around the central Cp*-Ir axis and rotation of the oxidized methyl functionalities about the C−C bonds.

RESULTS AND DISCUSSION

Direct MS Studies of the Activation of [Cp*Ir(pyalc)-OH], 1(OH). In previous work,[27] the resting state of the fully activated [Cp*Ir(chelate)X] precursor was proposed to be a bis-μ-oxo iridium(IV) dimer with two water molecules and one chelate ligand on each metal (Figure 1). However, only the reduced (III−III) form of this species without the aqua ligands has been observed in the gas phase from a reducing MALDI-MS matrix. Attempts to isolate this solution-phase species through atmospheric ionization and other solution phase techniques have proven difficult, but transient oxidized species are indeed observed in ESI mass spectra of solutions with low oxidant concentrations. This suggested they may play a role in the early formation of the active complex, and we undertook a mass spectrometry-based characterization study to probe the nature of these transient species. To determine which oxidized species are present at very low reaction times, reactive desorption electrospray ionization mass spectrometry (DESI-MS) was employed. In reactive DESI, charged microdroplets containing a reagent are directed toward a surface containing a reaction partner. Reactions are initiated on the surface and reactants, intermediates, and products are carried away from the surface in reflected secondary microdroplets which are intercepted by a mass spectrometer. These secondary microdroplets enter the heated capillary of the mass spectrometer where the solution phase reactions are evaporatively quenched within a few milliseconds of leaving the surface. This ambient ionization technique enables facile reaction studies of species applied to a surface and offers a unique approach to access the species present in solution in the early stages of the reaction. DESI-MS spectra of [Cp*Ir(pyalc)OH], **1(OH)**, were taken by depositing 10 μL of a 10 mM aqueous solution of **1(OH)** on paper affixed to a glass slide and then the surface was dried under a stream of N_2 before spraying it with water or aqueous solutions of $NaIO_{4(aq)}$ using a custom DESI source. In most cases, suitable ion intensity could be achieved without applying an electric potential to the source. No potential was applied to the source to avoid spurious oxidation of **1(OH)** by reactive oxygen species which can be generated by the electrochemical nature of the electrospray process.[37−39]

In the absence of oxidant, DESI-MS spectra of **1(OH)** almost exclusively contained the previously detected and structurally characterized ion $[Cp^*Ir(pyalc)]^+$, $[\mathbf{1}]^+$, (pyalc = 2-(2′-pyridyl)-2-propanolate m/z 464.1560) as the principal peak (Figure 2a).[36,40] Also detected in low abundance (less

dx.doi.org/10.1021/ic402390t | Inorg. Chem. 2014, 53, 423−433

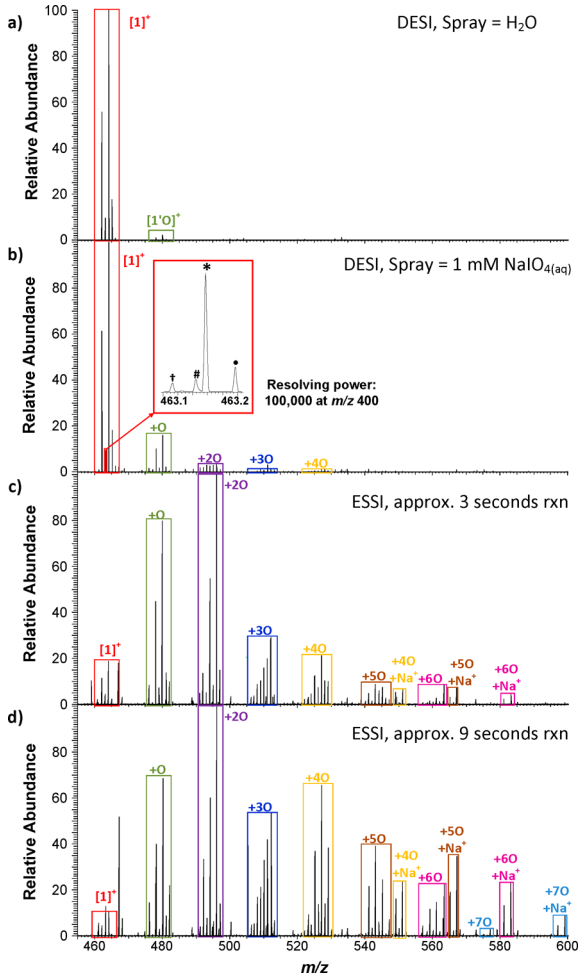

Figure 2. MS Spectra of **1(OH)**. Conditions: (a) DESI-MS of **1(OH)**, spray = H_2O. (b) DESI-MS of **1(OH)**, spray = 1 mM $NaIO_{4(aq)}$. Inset: zoom-in of 463.1−463.2 *m/z*. (c) ESSI-MS of 5 μM **1(OH)** + 50 μM $NaIO_{4(aq)}$, approximately 3 s reaction time. (d) ESSI-MS of 5 μM **1(OH)** + 50 μM $NaIO_{4(aq)}$, approximately 9 s reaction time. All spectra were collected at source voltage of 0 kV and are normalized to the most abundant peak. DESI-MS spectra were recorded using paper surfaces.

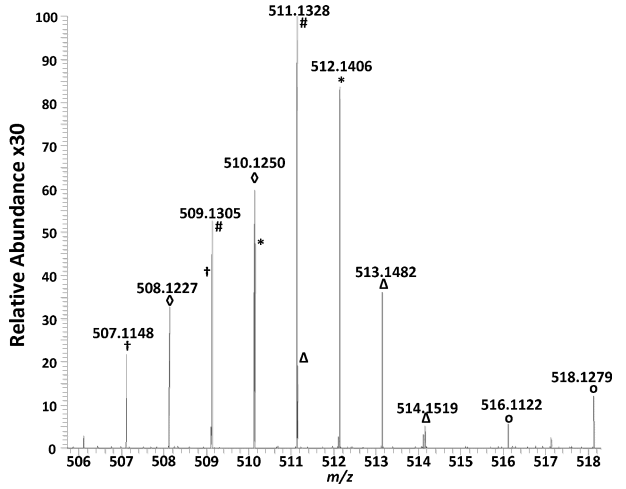

Figure 3. Highlighted $[\mathbf{1,O_3,}\text{-}\mathbf{H_m}]^+$ region of the DESI-MS spectrum in Figure 1b showing assigned intercalated peaks, with intercalated species indicated with the given symbols: * = $[\mathbf{1,O_3,}\text{-}\mathbf{H_0}]^+$, *m/z* 512.1406; **Δ** = $[\mathbf{1,O_3,}+\mathbf{H_1}]^+$, *m/z* 513.1483; # = $[\mathbf{1,O_3,}\text{-}\mathbf{H_1}]^+$, *m/z* 511.1328; ◇ = $[\mathbf{1,O_3,}\text{-}\mathbf{H_2}]^+$, *m/z* 510.1250; † = $[\mathbf{1,O_3,}\text{-}\mathbf{H_3}]^+$, *m/z* 509.1172; **o** = $[(\mathbf{1,O_2,}\text{-}\mathbf{H_1})\mathbf{Na}]^+$, *m/z* 518.1279.

than 3% relative to $[\mathbf{1}]^+$) were ions corresponding to the addition of a single oxygen atom to $[\mathbf{1}]^+$, $[\mathbf{1'O}]^+$ (*m/z* 480.1509), as well as H_2O (*m/z* 482.1666), NaOH (*m/z* 504.1485), HCl (*m/z* 500.1327), NaCl (*m/z* 522.1146), and $NaNO_2$ (*m/z* 533.1387) adducts of $[\mathbf{1}]^+$. The appearance of trace $[\mathbf{1'O}]^+$ was curious under these conditions, although a series of control experiments indicated that it was an artifact of the DESI process and unrelated to the compounds detected in the presence of oxidant (see Supporting Information for details).

When 1 mM $NaIO_{4(aq)}$ was used to spray a surface containing **1(OH)**, clusters of Ir-containing peaks were observed that arise from the oxidation of **1(OH)**. These species had a base molecular formula of $[\mathbf{1}]^+$ as well as 0 to 5 additional oxygen atoms and loss of 0 to 3 hydrogen atoms or gain of 1 hydrogen atom (Figures 2b, 3, and Supporting Information, Figure S1). We will refer to this set of oxidized species by the general notation $[\mathbf{1,O_n,}\text{-}\mathbf{H_m}]^+$, where **n** refers to the number of additional oxygen atoms and **m** refers to the number of lost hydrogen atoms from the base molecular formula of $[\mathbf{1}]^+$, $(C_{18}H_{25-m}O_{1+n}NIr)$. In the DESI-MS spectrum of **1(OH)** with 1 mM $NaIO_{4(aq)}$, $[\mathbf{1,O_n,}\text{-}\mathbf{H_m}]^+$ encompasses over 20 different Ir-containing compounds as well as cation and anion adducts of these species (See Figure 3 for representative data and Supporting Information, Table S1 for a list of the $[\mathbf{1,O_n,}\text{-}\mathbf{H_m}]^+$ compounds detected by DESI). A series of control studies, including ^{18}O labeling using 1 mM $NaIO_{4(aq)}$ in 97% $H_2{}^{18}O$ as the DESI spray (Supporting Information, Figure S2), confirmed that the $[\mathbf{1,O_n,}\text{-}\mathbf{H_m}]^+$ complexes observed were a direct result of the added periodate oxidant in the spray and not artifacts of the ionization process (see Supporting Information for details). With such a complex solution composition, it is clear that a high resolution instrument was required to identify and resolve the species present, as the isotopic profile of Ir caused many of the peaks to be intercalated. In fact, up to four species were found at the same nominal mass (*m/z* 463, Figure 2b, inset) but are well resolved in the orbitrap analyzer. Not unexpectedly, clusters of $Na_{x+1}(IO_4)_x{}^+$ are also observed in the DESI-MS when 1 mM $NaIO_{4(aq)}$ is used as the spray and, at higher concentrations of $NaIO_{4(aq)}$ or lower concentrations of **1(OH)** on the surface, these peaks dominate the spectrum.

Because the complete activation of **1(OH)** occurs in seconds, it is too fast to directly measure by taking aliquots of a reaction solution. However, the speciation in Figure 2b suggested the oxidation of **1(OH)** had only just begun under the short time scales of DESI. To gain time-resolved insight into the further oxidation of **1(OH)**, we constructed an online flow microreactor similar to a published design[29] that allowed us to study reactions between **1(OH)** and $NaIO_{4(aq)}$ at the seconds time scale when interfaced with an ESSI source (Supporting Information, Figures S3 and S4). In-tubing reaction times from approximately 3 to 20 s can be readily accessed by adjusting the residence time in the microreactor.

When 5 μM **1(OH)** is mixed online with 50 μM $NaIO_{4(aq)}$ in the micromixer and allowed to flow through the tubing for approximately 3 s prior to ionization, extensive oxidation of $[\mathbf{1}]^+$ to an approximately Poisson distribution of $[\mathbf{1,O_n,}\text{-}\mathbf{H_m}]^+$species is observed (Figure 2c). In fact, addition of up to 8 oxygen atoms is found under these conditions (See Supporting

dx.doi.org/10.1021/ic402390t | *Inorg. Chem.* 2014, 53, 423−433

Information, Table S2 for a complete list of $[\mathbf{1,O_n,-H_m}]^+$compounds detected by ESSI). Note that a potential was not applied to the ESSI source to observe these species. If a 5 kV potential were applied to the metal needle of a syringe containing **1(OH)** while flowing this solution directly into the ESSI source, small amounts of $[\mathbf{1,O_n,-H_m}]^+$ species were observed along with other unidentified Ir-containing species, even though no $NaIO_4$ was present in solution. This result indicated that an applied potential affects the electrochemical oxidation of **1(OH)** and alters the observed speciation of $[\mathbf{1,O_n,-H_m}]^+$, demonstrating an important advantage of ESSI in that it avoids this complication.

When the capillary tubing between the mixing tee and the ESSI source was extended to allow the solution to react in the tubing for 9 s, there was a significant shift in the observed speciation of $[\mathbf{1,O_n,m}]^+$compounds toward more oxidized species (Figure 2d). After approximately 15 s, no further change in speciation was observed, indicating that periodate had been expended and the reaction was exhausted. We suspect the bulk of reaction progress to have occurred in the tubing. Significant rate enhancement has been observed for some reactions in microdroplets as opposed to bulk solutions.[41,42] However, the significant shift in speciation relative to the DESI data and the observed dependence on residence time in tubing demonstrated that reactions, in this case, progressed to a significant extent in the flow system as opposed to the ESSI microdroplets.

The entire nonproductive induction period observed in water-oxidation with Cp*Ir precursors has been shown to consume about 20 equiv of $NaIO_4$, so it is not surprising that incomplete oxidation of **1(OH)** was observed under the applied conditions (10 equiv of $IO_{4(aq)}$). Unfortunately, increasing the concentration of $NaIO_{4(aq)}$ relative to **1(OH)** significantly decreased the intensity of the $[\mathbf{1,O_n,-H_m}]^+$ peaks in the mass spectra, even at increased concentrations of **1(OH)**. In fact, when 20 equiv of $NaIO_{4(aq)}$ were mixed online with 5 μM **1(OH)**, no Ir-containing peaks were observed. This was likely caused by competitive ionization between $Na_{x+1}(IO_4)_x^+$ clusters and the $[\mathbf{1,O_n,-H_m}]^+$ species, a common problem in electrospray ionization of analytes in electrolyte solutions.[43−45] We were unable to increase the concentrations of **1(OH)** or $NaIO_{4(aq)}$ any further without risking harm to the instrument through salt deposition, likely precluding the observation of more extensively oxidized species or the fully activated form of **1(OH)** by electrospray methods. Neutral oxidants would avoid this competitive ionization, and H_2O_2 has been shown to degrade Cp* in similar complexes.[24] Preliminary experiments where 5 μM **1(OH)** was mixed online with 100 μM H_2O_2 and sprayed through an ESSI source gave very similar spectra as Figure 2c. This implied that the early stages of this oxidation are similar with either H_2O_2 and $NaIO_{4(aq)}$; however, because this neutral oxidant is unable to drive catalytic water oxidation or C−H hydroxylation, the later stages of precatalyst activation must diverge.[46]

While many different structures are possible for each $[\mathbf{1,O_n,-H_m}]^+$ species detected (vide infra), the mechanism for their production most consistent with the observed data consists of a sequence of consecutive nonselective oxidations of Cp*. The complete set of $[\mathbf{1,O_n,-H_m}]^+$ peaks can be rationalized by considering the range of Ir(III) and Ir(IV) complexes that could be present during the successive oxidation of the Cp* ligand, where Cp* methyl groups are initially hydroxylated and then oxidized further to aldehyde and carboxylate groups (Figure 4). See Supporting Information, Figure S5 for a set of representative isomers for up to n = 3. This scheme accounts

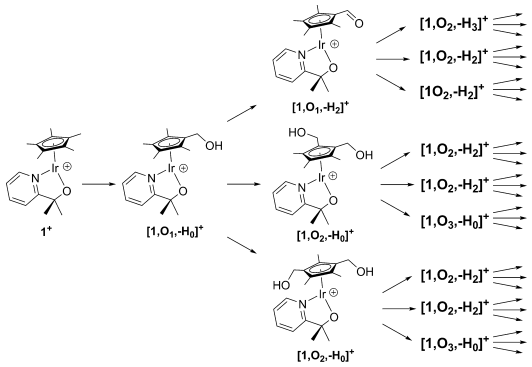

Figure 4. Potential initial pathways for Cp* oxidation. Each arrow indicates a formal $2e^-$ oxidation.

for both the successive addition of oxygen atoms as well as loss of hydrogen atoms in the observed $[\mathbf{1,O_n,-H_m}]^+$ compounds, where oxidation of an alcohol or carboxylation leads to a formal loss of hydrogen atoms. Eventually, the Cp* ligand would either become sufficiently electron-deficient to dissociate from Ir or would undergo complete degradation within the metal's coordination sphere to acetate, CO_2, or other organic products. The previous detection of one- and two-carbon fragments means that at some point the C═C bonds of the 5-membered ring must be oxidatively cleaved;[27] however, the statistical distribution of $[\mathbf{1,O_n,-H_m}]^+$ species and intensity of $[\mathbf{1,O_1,-H_0}]^+$ relative to the other species suggests that for **1(OH)** in the presence of $NaIO_{4(aq)}$, $[\mathbf{1,O_1,-H_0}]^+$ is the prominent entry into precatalyst activation to generate the observed $[\mathbf{1,O_n,-H_m}]^+$ under the employed conditions.

The complexity of the observed speciation strongly suggests that this process does not follow a specific pathway. Almost every iterative combination of **m** and **n** was detected for **n** = 2−4 oxygen atoms and **m** = 0−3 hydrogen atoms. Although it is difficult to relate ESI-MS intensities to concentrations in complex mixtures, it is unlikely for the sensitivity to vary drastically between related $[\mathbf{1,O_n,-H_m}]^+$ compounds (i.e., more than an order of magnitude). Furthermore, for **n** = 3 and greater, species with an additional hydrogen atom, e.g., $[\mathbf{1,O_3,+H_1}]^+$, were detected which is most easily rationalized by the addition of a hydroxyl or hydroperoxyl group to quaternary carbons of previously oxygenated Cp* rings, as suggested by NMR studies of related complexes using hydrogen peroxide as the terminal oxidant (see representative structures for $[\mathbf{1,O_3,+H_1}]^+$ in Supporting Information, Figure S5).[24] Another possibility is hydroxide/water coordination to Ir or the formation of strongly bound solvent adducts of these more polar species. This suggests that Ir-coordination isomers should also be considered for the observed $[\mathbf{1,O_n,-H_m}]^+$ peaks (in addition to those in Supporting Information, Figure S5). Given the complexity of these spectra, there is no reason to assume that a particular $[\mathbf{1,O_n,-H_m}]^+$ peak represents only one isomer of Cp* oxidation and/or Ir-coordination, and it is likely that multiple isomers are present for each molecular formula (vide infra). Finally, at high values of **n** (i.e., **n** = 6 and 7), the number of different values of **m** observed decreases and only $+\mathbf{H_1}$, $-\mathbf{H_0}$, $-\mathbf{H_1}$ species are observed. This reflects the lower number of potential compounds that can stochastically be formed at this later stage of oxidation. It is not clear if the various oxidation

dx.doi.org/10.1021/ic402390t | Inorg. Chem. 2014, 53, 423−433

pathways converge, or if only certain pathways can access addition of these higher numbers of oxygen atoms prior to Cp* dissociation.

These results differ from those of recent NMR studies by Macchioni and co-workers[24,47] which examined the less active precatalyst [Cp*Ir(2-benzoylpyridine)NO_3] using H_2O_2 or ceric ammonium nitrate (CAN) as the oxidant. They showed compelling evidence for initial oxo-functionalization of a quaternary carbon on Cp* to form hydroxyl or hydroperoxyl substituted Cp* rings.[24,47] These species would correspond to $[\mathbf{1,O_1,+H_1}]^+$ or $[\mathbf{1,O_2,+H_1}]^+$ which were not observed in the DESI or ESSI spectra under our conditions. Given the preliminary studies performed using H_2O_2 described above, it is unlikely that the differing conclusions are a result of the different oxidants. Instead, we propose that the electron donating properties of our pyalc ligand relative to the electron withdrawing 2-benzoylpyridine ligand causes this change in reactivity. To confirm the inherent difference in reactivity between **1(OH)** and the 2-benzoylpyridine catalyst, 3 equiv of $NaIO_{4(aq)}$ were added to a solution of **1(OH)** in D_2O and ^1H NMR spectra were acquired, which showed the expected formation of acetate as well as a broad hump in the baseline in the ppm range of Cp* and pyalc methyl signals (see Supporting Information, Figure S6). A few small peaks indicating some relatively minor species are present, but these peaks were not stable over a 4 h period and did not give any observable cross peaks in NOESY spectra, precluding their assignment. These NMR studies indicate that no abundant diamagnetic Ir species are formed when **1(OH)** is exposed to $NaIO_{4(aq)}$, supporting the complex speciation that was resolved by the present MS studies.

Structural Characterization of Oxidized Ir(Cp*)(pyalc)$^+$ Complexes $[\mathbf{1,O_{1,2},-H_0}]^+$. Given the complexity and number of species detected in the MS spectra of **1(OH)**, we focused our efforts on the identification of the initial oxidation products $[\mathbf{1,O_{1,2},-H_0}]^+$ to critically evaluate the mechanism proposed above (see Figure 4). Unfortunately, tandem MS fragmentation studies (MS/MS) could not allow us to distinguish between any of the six likely structures for $[\mathbf{1,O_1,-H_0}]^+$ (see Figure 5), which includes C−H hydroxylation of Cp* or the pyalc ligand $[\mathbf{1,O_1,-H_0}]^+_{A\text{-}C}$, Cp* epoxidation $[\mathbf{1,O_1,-H_0}]^+_D$, an Ir(V)-oxo $[\mathbf{1,O_1,-H_0}]^+_E$, and formal loss of a hydride from Cp* to generate the fulvene species $[\mathbf{1,O_1,-H_0}]^+_F$. Oxygen-insertions into the pyalc ligand to give bound peroxide or N-oxide species were ruled unlikely by the continuous series of +O−H functionalizations observed.

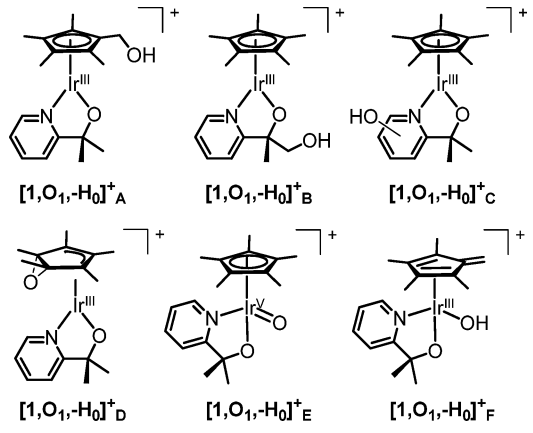

Figure 5. Potential Structures for $[\mathbf{1,O_1,-H_0}]^+$ (representative isomers shown).

We further ruled out $[\mathbf{1,O_1,-H_0}]^+_C$ as a likely candidate for two reasons: (1) there is no reasonable way to explain either the number of observed additional oxygen atoms or the loss of hydrogen atoms, and (2) **1(OH)** was found to be incapable of arene hydroxylations in previous C−H oxidation studies.[23,46] $[\mathbf{1,O_1,-H_0}]^+_B$ was ruled out by a selective isotope labeling study. A pyalc ligand with fully deuterated methyl groups was synthesized and used to prepare $\mathbf{d_6}$-**1(OH)**, analogously to **1(OH)** (see Supporting Information). DESI-MS spectra of $\mathbf{d_6}$-**1(OH)** using 1 mM $NaIO_{4(aq)}$ as the spray were qualitatively the same as those for **1(OH)**, except that the masses were shifted by 6 amu (Supporting Information, Figure S7). The set of observed $[\mathbf{d_6\text{-}1,O_n,\text{-}H_m}]^+$ compounds showed no evidence for loss of deuterium, indicating that the methyl groups of d_6-pyalc are resistant to hydroxylation under these conditions. As mentioned above, MS/MS data of $[\mathbf{1,O_n,\text{-}H_m}]^+$ and $[\mathbf{d_6\text{-}1,O_n,\text{-}H_m}]^+$ compounds were uninformative as all of the detected fragments were from the pyalc and d_6-pyalc ligands rather than from Cp* as exemplified by the fragmentation of $[\mathbf{d_6\text{-}1,O_1,\text{-}H_0}]^+$ and $[\mathbf{1,^{18}O_1,\text{-}H_0}]^+$ compared to $[\mathbf{1,O_1,\text{-}H_0}]^+$ (Supporting Information, Figure S8).

The remaining structures could be classified by whether or not they contained a hydroxyl group (with −OH: $[\mathbf{1,O_1,-H_0}]^+_A$ and $[\mathbf{1,O_1,-H_0}]^+_F$; without −OH: $[\mathbf{1,O_1,-H_0}]^+_D$ and $[\mathbf{1,O_1,-H_0}]^+_E$), which would show distinct differences in the vibrational spectrum of the $[\mathbf{1,O_1,-H_0}]^+$ ion. Furthermore $[\mathbf{1,O_1,-H_0}]^+_A$ and $[\mathbf{1,O_1,-H_0}]^+_F$ contain many of the same functionalities and differ only by the position of the OH and the introduction of a CH_2 group in $[\mathbf{1,O_1,-H_0}]^+_F$. This presented an ideal opportunity for utilizing cryogenic ion vibrational predissociation (CIVP) to obtain the structural information needed to support the initial oxidation mechanism of the precatalyst **1(OH)**. The overall character of the vibrational bands in this class of molecules was already considered in a report[36] of the $[\mathbf{1}]^+\cdot\mathbf{D_2}$ cryogenic ion vibrational predissociation (CIVP) spectrum reproduced in Figure 6d. This band pattern was assigned to a series of fundamental excitations (as indicated) based on an accurate prediction of their locations and relative intensities by harmonic calculations at the cam-B3LYP/SDD/6-311+G(d,p) level. A qualitative overview of the spectrum reveals three strong CH_2 and CH_3 stretches between 2900 and 3000 cm^{-1}, as well as a few weak transitions near 3100 cm^{-1} corresponding to CH stretches on the pyridine ring. Moving to lower energy, we find a more congested series of transitions that correspond to normal modes derived from collective motions of many atoms. Two pyridine stretching modes lie at 1618 cm^{-1} and 1481 cm^{-1}, while the CH_3 bending and rocking fundamentals appear at 1457 cm^{-1} and 1022 cm^{-1}, respectively. Finally, the C−O stretching motion, coupled to CH and CH_3 bends, yields a suite of transitions at 1165, 1112, and 969 cm^{-1}, respectively. We would expect a significant response in both the CH stretch and fingerprint regions if the first oxidized product $[\mathbf{1,O_1,-H_0}]^+$ contained a fulvene functionality, as it is predicted to break the planar symmetry of the Cp* ligand and introduce an sp^2 carbon (Supporting Information, Figure S9). Indeed, harmonic calculations predicted distinct differences in the vibrational spectra of the alternative structures and thus presented an opportunity to distinguish between these potential isomers.

The infrared predissociation spectrum of $[\mathbf{1,O_1,-H_0}]^+$ is presented in Figure 6c. Overall, the vast majority of the

dx.doi.org/10.1021/ic402390t | Inorg. Chem. 2014, 53, 423−433

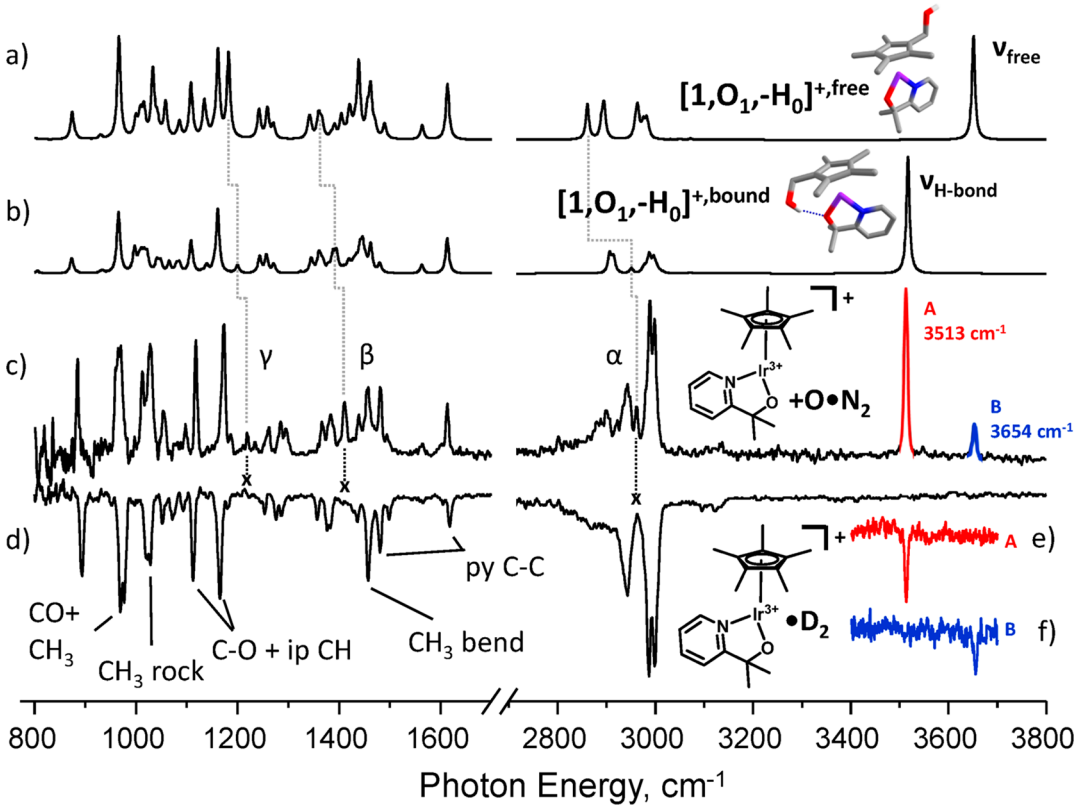

Figure 6. Harmonic spectra (at the cam-B3LYP/SDD/6-311+G(d,p) level, scaling factors given in experimental) of two isomers of the $[\mathbf{1,O_1,\text{-}H_0}]^+$ complex which differ according to whether the OH on the Cp* ring is free (a) or engaged in an intramolecular H-bond (b). The experimental predissociation spectrum of $[\mathbf{1,O_1,\text{-}H_0}]^+\cdot\mathbf{N_2}$ is presented in (c). The infrared predissociation spectrum of $[\mathbf{1}]^+$, collected in an earlier study,[5] is reproduced in trace (d), inverted for comparison. In addition to two new OH stretches, only three new transitions appear upon oxidation and are labeled α, β, and γ. The x's in trace (d) indicate that these transitions are not present in unoxidized $[\mathbf{1}]^+$. Using the IR^2MS^3 photochemical hole-burning method, the two OH transitions in the experimental spectrum were confirmed to originate from two different isomers, as evidenced by the mutually exclusive dips in the holeburning spectra of $[\mathbf{1,O_1,\text{-}H_0}]^+\cdot\mathbf{N_2}$ given in the red and blue traces (e) and (f).

transitions are retained upon oxidation, with the most obvious addition corresponding to the two distinct OH stretches at 3513 and 3654 cm^{-1}, which are entirely absent in the parent compound $[\mathbf{1}]^+$. This rules out $[\mathbf{1,O_1,\text{-}H_0}]^+_D$ and $[\mathbf{1,O_1,\text{-}H_0}]^+_E$ as potential structures, leaving the alcohol $[\mathbf{1,O_1,\text{-}H_0}]^+_A$ and the fulvene $[\mathbf{1,O_1,\text{-}H_0}]^+_F$ as the remaining possible structures. In addition, new peaks, labeled α, β, and γ, also appear lower in energy at 2961, 1410, and 1217 cm^{-1}, respectively. The overall preservation of the spectrum upon oxidation strongly suggests that the structure of this species is not significantly perturbed from that of $[\mathbf{1}]^+$, as would be expected for the $[\mathbf{1,O_1,\text{-}H_0}]^+_A$ isomer. However, as only one oxygen atom was added to this species, the presence of two OH stretches could not be readily explained by a single isomer.

Photochemical hole burning using the IR^2MS^3 method was employed to investigate the origin of the two sharp bands in the region expected for OH stretching fundamentals, denoted A and B in Figure 6. The results are shown as negative going peaks (resulting from dips in the probe signal) in panels (e) and (f) in Figure 6. The fact that only one OH transition appears in each dip spectrum unambiguously assigns these features to two distinct isomers. The more red-shifted band at 3513 cm^{-1} is consistent with formation of a donor H-bond and the other higher in energy at 3654 cm^{-1} occurs in the location expected for a free OH. These results, paired with the preservation of the main band structure upon oxidation, were used to guide a theoretical structural search. The calculated structures of the two lowest energy isomers are given in Figure 6a and 6b along with their (scaled) harmonic spectra. Both structures correspond to hydroxylation of Cp* methyl groups. The lowest energy structure $[\mathbf{1,O_1,\text{-}H_0}]^{+,bound}$ is that displayed in Figure 6b, and features an intramolecular H-bonded arrangement in which the hydroxyl group attaches to the oxygen atom of the pyalc ligand. Comparison with the harmonic spectrum of the bare complex $[\mathbf{1}]^+$ (Supporting Information, Figure S10) gives a structural basis for the three new transitions (α, β, γ in trace 6c). The α transition corresponds to asymmetric stretching of the CH_2 functionality on the oxidized Cp* carbon, while the β and γ transitions are traced to OH bends coupled to CH_2 bends and twists. As these new transitions all correspond to motions involving the CH_2OH functionality, this further supports the structural assignment as oxidation on the Cp* ligand.

A second rotamer $[\mathbf{1,O_1,\text{-}H_0}]^{+,free}$, depicted in Figure 6a, lies 3.0 kcal/mol higher in energy (at the cam-B3LYP/SDD/6-311+G(d,p) level) and features a free OH moiety, generated through simple rotation of the monohydroxylated Cp* ligand around the Cp*-Ir axis. Modes with the same qualitative character as those identified as α, β, and γ are indicated with gray dotted lines, and all redshift upon breaking the intramolecular hydrogen bond. We note that at room temperature in solution, rotation of the unmodified Cp* ligand is very fast on the NMR time scale,[20] but at the lower temperature and isolated environment of the CIVP experiment,

dx.doi.org/10.1021/ic402390t | Inorg. Chem. 2014, 53, 423−433

it is not surprising that functionalized Cp* rotamers can be trapped. Interestingly, although its OH stretch feature is weaker, the equilibrium population of the higher (3.0 kcal/mol) energy isomer responsible for that band should not be significantly populated at the trap temperature of approximately 30 K. As such, there is likely a sufficiently high barrier separating the rotamers such that that either can be trapped as the ion is slowly cooled by buffer gas collisions. Such trapped higher energy isomers have been observed in previous studies of small peptides,[31] and the formation mechanisms and cooling dynamics are presently in a rather primitive state of characterization. Though this energy difference is too large to explain the relative absolute abundances of the two isomers (5:1 assuming roughly equal transition strength of the two OH's), it does qualitatively track the observed trend, with the hydrogen-bond stabilized structure in higher abundance.

The similarity of the $[\mathbf{1,O_1,\text{-}H_0}]^+$ and $[\mathbf{1}]^+$ vibrational spectra, supported by calculations of low lying structures and harmonic spectra, provide compelling evidence for the occurrence of forms $[\mathbf{1,O_1,\text{-}H_0}]^{+,\text{bound}}$ and $[\mathbf{1,O_1,\text{-}H_0}]^{+,\text{free}}$ for the $[\mathbf{1,O_1,\text{-}H_0}]^+$ ion, but it is useful to consider the possible role of the fulvene compound $[\mathbf{1,O_1,\text{-}H_0}]^+_F$ contributing to the ion ensemble. The same level of calculation used above places this species considerably higher (34 kcal/mol) in energy, compared to the metastable $[\mathbf{1,O_1,\text{-}H_0}]^{+,\text{free}}$ form. More importantly, the harmonic vibrational spectrum of $[\mathbf{1,O_1,\text{-}H_0}]^+_F$ is clearly distinct from $[\mathbf{1,O_1,\text{-}H_0}]^+$ in the region near the $=CH_2$ bending vibration near 1500 cm^{-1} in the fingerprint region as explicitly demonstrated in Supporting Information, Figure S11. We therefore confidently conclude that the first oxidation product $[\mathbf{1,O_1,\text{-}H_0}]^+$ occurs with formation of a hydroxyl group on the Cp* ring $[\mathbf{1,O_1,\text{-}H_0}]^+_A$, yielding one isomer which is observed in the gas phase as two rotamers of the functionalized ring.

To support the nonselective oxidation mechanism proposed in Figure 4, we extended the spectroscopy study to the species formally corresponding to addition of a second oxygen atom to the $[\mathbf{1}]^+$ complex, denoted $[\mathbf{1,O_2,\text{-}H_0}]^+$, and present the CIVP spectrum of the N_2 tagged $[\mathbf{1,O_2,\text{-}H_0}]^+\cdot\mathbf{N_2}$ ion in Figure 7 along with that of $[\mathbf{1,O_1,\text{-}H_0}]^+\cdot\mathbf{N_2}$ (inverted) for comparison. Unfortunately, the suspected aldehyde, $[\mathbf{1,O_2,\text{-}H_2}]^+$, could not be generated in sufficient abundance to gather a good CIVP spectrum. The most significant spectral responses to the second oxidation step are the *preservation* of the two OH bands assigned above in the $[\mathbf{1,O_1,\text{-}H_0}]^+$ spectrum (denoted A in Figure 7d) as well as the appearance of two closely spaced bands (B in Figure 7d) just below the most intense OH feature in the $[\mathbf{1,O_1,\text{-}H_0}]^+$ spectrum. The A transitions lie within 5 cm^{-1} of those observed for the single oxygen complex $[\mathbf{1,O_1,\text{-}H_0}]^+$, while the B features occur at 3471 and 3436 cm^{-1} and are broader than those in A (8 cm^{-1} fwhm) by 4 to 6 cm^{-1}. The redshift and broadening of OH transitions is typical for OH oscillators engaged in stronger H-bonds, and are common indicators of strong hydrogen bonding, suggesting two OH groups are involved in stronger H-bonds than the single H-bonding motif present in $[\mathbf{1,O_1,\text{-}H_0}]^+$ (i.e., to the oxygen atom of the pyalc ligand). No significant response in the fingerprint region is observed upon the second oxidation (Supporting Information, Figure S12), as all three characteristic transitions transitions (i.e., α, β, and γ in Figure 6) are still present and no fulvene CH_2 stretch is observed.

As the $[\mathbf{1,O_2,\text{-}H_0}]^+$ complex only contains two additional oxygen atoms, the presence of four OH transitions strongly suggests the presence of multiple isomers. Infrared double resonance (IR^2MS^3) was therefore once again employed to establish both the existence of isomers as well as identify the independent band patterns. The resulting ion dip spectra are displayed at the right of Figure 7c, revealing the distinct spectral patterns of two isomers. Interestingly, one of these isomers has both bands (A) that were associated with the two different rotamers in $[\mathbf{1,O_1,\text{-}H_0}]^+$. This suggests that this isomer of $[\mathbf{1,O_2,\text{-}H_0}]^+$ accommodates the oxygen atoms in both positions on the Cp* ring, one with an OH group bound to the pyridine alkoxy ligand while the second OH is nonbonded. This implies that the second isomer occurs in a configuration in which both OH groups are engaged in strong H-bonds.

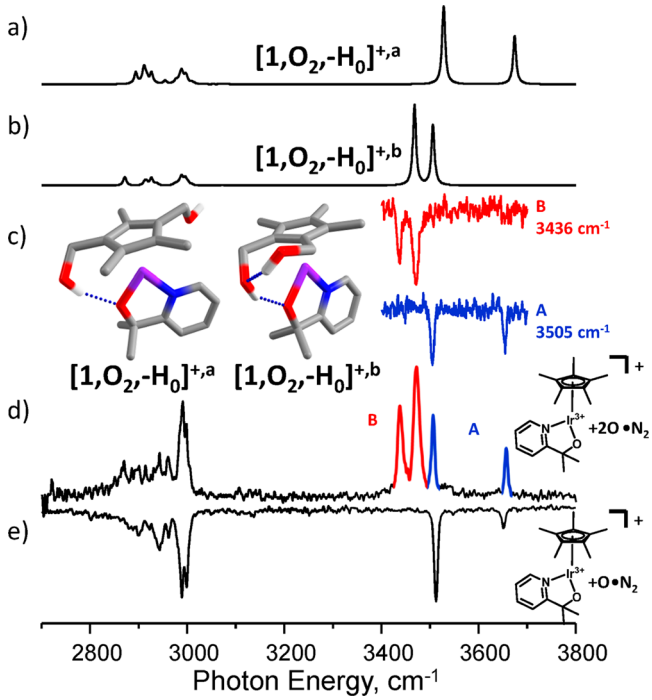

Figure 7. (a, b) Harmonic spectra (cam-B3LYP/SDD/6-311+G(d,p) level, scaling factors given in experimental) of two isomers of the $[\mathbf{1,O_2,\text{-}H_0}]^+$ complex which differ according to whether their Cp* ligand has one free OH (a), or two intramolecular H-bound OH functionalities (b). The calculated structures of the two isomers are given at the left of panel (c). The experimental predissociation spectrum of $[\mathbf{1,O_2,\text{-}H_0}]^+\cdot N_2$ is presented in (d). The IR^2MS^3 photochemical hole-burning method (see text),[3] establishes that the four OH transitions in the experimental spectrum originate from two different isomers, as evidenced by the mutually exclusive dips in the inverted red and blue traces at the right of (c). The (inverted) infrared predissociation spectrum of $[\mathbf{1,O_1,\text{-}H_0}]^+\cdot N_2$ is presented in panel (e).

Having identified the spectra of the two $[\mathbf{1,O_1,\text{-}H_0}]^+$ rotamers, we carried out a computational isomer search, which recovered two low-energy local minima with structures and energies shown at the left in panel (c). Harmonic spectra for these structures are also displayed and accurately account for the two bands in the OH stretching region. The first structure, denoted $[\mathbf{1,O_2,\text{-}H_0}]^{+,a}$, where "meta" methyl groups are hydroxylated, indeed occurs with the hydroxyl groups in the two locations occupied independently in the $[\mathbf{1,O_1,\text{-}H_0}]^{+,\text{bound}}$ and $[\mathbf{1,O_1,\text{-}H_0}]^{+,\text{free}}$ compounds. Note that the intensity of the free OH is much closer to that of the bound transition, unlike that of $[\mathbf{1,O_1,\text{-}H_0}]^+$, where the weak free −OH transition is proposed to arise from the lower population of the $[\mathbf{1,O_1,\text{-}H_0}]^{+,\text{free}}$ isomer in the ion packet, relative to $[\mathbf{1,O_1,\text{-}H_0}]^{+,\text{bound}}$.

dx.doi.org/10.1021/ic402390t | *Inorg. Chem.* 2014, 53, 423−433

This suggests constitutional rather than rotational isomerism. The structure which accurately accounts for the B features, $[\mathbf{1,O_2,\text{-}H_0}]^{+,b}$, where "ortho" methyl groups are hydroxylated, is depicted at the right in Figure 7c, and is calculated to lie only 0.3 kcal/mol above $[\mathbf{1,O_2,\text{-}H_0}]^{+,a}$ suggesting that there is little to no thermodynamic driving force for "ortho" vs "meta" substitution of C−H groups on Cp*. The fact that the band due to the ligand-bound OH is red-shifted in this so-called "homodromic" or pseudolinear acceptor−donor configuration is clearly due to the cooperative effect of the second OH,[48] which strengthens the initial H-bond to the ligand. A third $[\mathbf{1,O_2,\text{-}H_0}]^{+}$ structure, with both OH functionalities H-bonded to the pyridine alkoxide, was also calculated to be a local minimum, but its harmonic spectrum only displayed a single intense OH transition due to nearby symmetric and asymmetric OH stretches (Supporting Information, Figures S12 and S13). In addition to confirming the initial steps for the oxidation of **1(OH)** proposed in Figure 4, the vibrational spectrum of $[\mathbf{1,O_2,\text{-}H_0}]^{+}$ further highlights the essentially nonselective nature of the functionalization of Cp* ligand of **1(OH)**, where C−H hydroxylation of $[\mathbf{1,O_1,\text{-}H_0}]^{+}$ can occur at any methyl group without any apparent direction and in competition with further oxidation of the initial hydroxyl group to generate $[\mathbf{1,O_2,\text{-}H_2}]^{+}$, all of which were directly observed in this study.

Activation of Other Catalyst Precursors. Preliminary MS studies on other catalyst precursors were undertaken to investigate the nature of these oxidized species. [Cp*Ir(ppy)-OH] (ppy = 2-phenylpyridine), **2(OH)**, was studied to interrogate the role of the supporting ligand. As expected from previous studies,[27] the oxidation of **2(OH)** proceeded slower than that of **1(OH)**. When DESI-MS spectra of **2(OH)** were taken analogously to those of **1(OH)**, very little oxidation of **2(OH)** was observed (Supporting Information, Figure S14). When the concentration of **2(OH)** on the surface was reduced by depositing 10 μL of a 1 mM dichloromethane or methanol solution of **2(OH)** on a hydrophobic porous PTFE surface and 1 mM $NaIO_{4(aq)}$ was sprayed, oxidation of **2(OH)** was more evident (Supporting Information, Figure S15a).[49] Online reaction monitoring showed similar results (Supporting Information, Figure S15b), where oxidation of **2(OH)** generated similar $[\mathbf{2,O_n,\text{-}H_m}]^{+}$ species as **1(OH)**; however, the oxidation was less extensive at the same time points. These results are consistent with the observed slower oxidation of **2(OH)** relative to **1(OH)** and with the Cp* moiety of **1(OH)** and **2(OH)** being oxidized.[27]

MS/MS data for **2(OH)** was more informative than for **1(OH)**. When $[\mathbf{2}]^{+}$ was isolated and subjected to collision induced dissociation (CID) in the ion trap of the LTQ-Orbitrap instrument, the fragments corresponded to loss of neutral H_2, H_4, and H_6, suggesting sequential loss of H_2 from the Cp* ring (Supporting Information, Figure S16a). However, when $[\mathbf{2,O_2,\text{-}H_0}]^{+}$ was subjected to CID the principal fragment corresponded to loss of neutral CH_4O; other significant neutral losses included CH_2O, $C_2H_4O_2$, H_2, and H_4 (Supporting Information, Figure S16b). While assignment of structures to the charged fragments is not possible with only this data, these results suggest that the additional oxygen atoms are closely associated with the methyl groups of the Cp* ring, given that the ppy ligand cannot reasonably provide the number of carbon and hydrogen atoms that are lost with each oxygen atom. These studies indicate that the mode of activation of **2(OH)** is very similar to that of **1(OH)**, although it is slower. Furthermore, the nonstatistical distribution of $[\mathbf{2,O_n,\text{-}H_m}]^{+}$ speciation in Supporting Information, Figure S15b relative to $[\mathbf{1,O_n,\text{-}H_m}]^{+}$ in Figure 2c suggests that the supporting ligand influenced the course of Cp* oxygenation.

The neutral (cod)Ir(pyalc) complex **3** is also an effective precatalyst for water oxidation, and has been shown to exhibit catalytic activity similar to **1(OH)**, despite that the Cp* ligand is not present.[27] We studied the activation of **3** under exposure to $NaIO_{4(aq)}$ to indirectly support that the Cp* ligand of **1(OH)** is oxidized during activation, as well as gain information on the mode of activation of **3**. The species **3** is not stable in air-saturated solutions and required more sensitive handling, but good DESI-MS spectra could be obtained (see Methods and Supporting Information, Figure S17a). As expected, exposing **3** to $NaIO_{4(aq)}$ produced drastically different MS spectra than **1(OH)** (Supporting Information, Figure S17b). When 1 mM $NaIO_{4(aq)}$ is used as the spray, $[\mathbf{3,O_1,+H_1}]^{+}$ species is the largest Ir-containing peak, with almost no further oxidation observed in the DESI-MS spectrum. This species is ^{18}O-labeled when 1 mM $NaIO_{4(aq)}$ is used as the spray (Supporting Information, Figure S18). Unfortunately, the sensitivity of **3** to air precluded its measurement by ESSI. The structure of $[\mathbf{3,O_1,+H_1}]^{+}$ is currently unknown. However, the fact that it is by far the most abundant oxidized species indicates that the mode of precatalyst activation has been fundamentally altered. The previous detection of traces of the cod-bis-epoxide as well as succinic acid in solutions of fully oxidized **3**[27] are consistent with an epoxidation pathway, leading to dissociation and further oxidative cleavage of the epoxidized cod ligand. Unfortunately, despite that less than 10 equiv of sodium periodate would be required to activate **3**, ESSI-MS of solutions prepared by mixing 10 equiv of $NaIO_{4(aq)}$ with **3** and allowing the reaction to complete before diluting to 10 μM Ir and directly infusing this solution did not show any Ir-containing peaks that did not contain a cod ligand. Importantly, when $\boldsymbol{d_6}$**-3** bearing the d_6-pyalc ligand was used under the same conditions, virtually identical spectra were obtained at +6 higher m/z values, demonstrating that also in the cod precursors the chelate ligand remains unaltered at least during the initial stage of activation.

■ CONCLUSIONS

By using multiple direct MS methods which probe the speciation of **1(OH)** as it changes under conditions directly relevant to catalysis, we present significant evidence that precatalytic activation of **1(OH)** by periodate occurs through consecutive, nonselective hydroxylations and oxidations of the Cp* ligand. This is likely followed by oxidative cleavage of the ring of Cp* to yield CO_2 and small organic acid byproducts such as acetic acid. Furthermore, we did not find any evidence for oxyfunctionalization of the supporting chelate ligand under the applied conditions. To confirm the structural assignments and support the proposed mechanism, the initial oxidation products have been characterized by their exact mass, their fragmentation pattern, isotope labeling of selected groups/solvent, and their vibrational spectra in the gas phase. Somewhat surprisingly, all data suggest that this process does not follow a unique pathway, but rather a highly complex competition between the available hydroxylations, dehydrogenations, and carboxylations of Cp*. This process leads to a large array of species which we speculate collapses to yield the previously proposed[27] dimer $[Ir^{IV}(pyalc)(H_2O)_2(\mu\text{-}O)]_2^{2+}$. Furthermore, comparing the activation of **1(OH)** to previous

dx.doi.org/10.1021/ic402390t | Inorg. Chem. 2014, 53, 423−433

studies[24,47] and the related compound **2(OH)** suggests that the supporting ligand plays a significant role in modulating the activation of half-sandwich Cp*Ir oxidation catalysts. Also, some insight has been gained in the activation of the related cod precursors.

Although the different methods brought to bear on these systems have yielded much information about organometallic Ir catalyst activation, the active catalytic species for water oxidation or C−H hydroxylation have yet to be identified and structurally characterized. Nevertheless, this study presents a detailed picture of speciation during precursor transformation for this class of Ir catalysts under oxidizing conditions which should be informative for the design of ligands for oxidation catalysts as well as the fundamental reactivity of metal-bound organic compounds.

■ ASSOCIATED CONTENT

Supporting Information

Further details are given in Figures S1−S18 and Tables S1−S4. This material is available free of charge via the Internet at http://pubs.acs.org.

■ AUTHOR INFORMATION

Corresponding Authors

*E-mail: mark.johnson@yale.edu (M.A.J.).
*E-mail: zare@stanford.edu (R.N.Z.).

Notes

The authors declare no competing financial interest.

■ ACKNOWLEDGMENTS

The Zare lab gratefully acknowledges the financial support from a subcontract with the University of Utah (Agreement # 10029173-S2) for which the Air Force Office of Scientific Research (Grant FA9550-12-1-0481) is the prime sponsor. M.A.J. and A.B.W. thank the Air Force Office of Scientific Research for support under Grant FA9550-09-1-0139. C.J.J. gratefully acknowledges support from the National Science Foundation American Competitiveness in Chemistry Fellowship (Grant CHE-1137404). A.J.I. is grateful for a Robert M. Bass and Anne T. Bass Stanford Graduate Fellowship and a National Science Foundation Graduate Research Fellowship. C.F. thanks the Center for Molecular Analysis and Design (CMAD) at Stanford for a Postdoctoral Fellowship. J.Z. thanks the China Scholarship Council affiliated with the Ministry of Education of China (Grant No. 201206010110). U.H. thanks the Alexander von Humboldt Foundation for a Feodor Lynen Research Fellowship, supplemented by a grant from the Yale Institute for Nanosciences and Quantum Engineering, and the Centre for Sustainable Chemical Technologies at the University of Bath for a Whorrod Research Fellowship. We would also like to thank Robert M. Waymouth and Hayley A. Brown for fruitful discussions.

■ REFERENCES

(1) Adlhart, C.; Chen, P. *Helv. Chim. Acta* **2000**, *83*, 2192−2196.
(2) Eberlin, M. N. *Eur. J. Mass Spectrom.* **2007**, *13*, 19−28.
(3) *Reactive Intermediates: MS Investigations in Solution*; Santos, L. S., Ed.; Wiley-VCH: Weinheim, Germany, 2010.
(4) McIndoe, J. S. *Spectroscopic Properties of Inorganic and Organometallic Compounds*; Yarwood, J., Douthwaite, R., Duckett, S., Eds.; Royal Society of Chemistry: Cambridge, U.K., 2010; Vol. *41*.
(5) Zhu, W.; Yuan, Y.; Zhou, P.; Zeng, L.; Wang, H.; Tang, L.; Guo, B.; Chen, B. *Molecules* **2012**, *17*, 11507−11537.
(6) Santos, L. In *Reactive Intermediates*; Santos, L. S., Ed.; Wiley-VCH: Weinheim, Germany, 2010; pp 133−198.
(7) Coelho, F.; Eberlin, M. N. *Angew. Chem., Int. Ed.* **2011**, *50*, 5261−5263.
(8) Vikse, K. L.; Ahmadi, Z.; Manning, C. C.; Harrington, D. A.; McIndoe, J. S. *Angew. Chem., Int. Ed.* **2011**, *50*, 8304−8306.
(9) Takáts, Z.; Wiseman, J. M.; Gologan, B.; Cooks, R. G. *Science* **2004**, *306*, 471−473.
(10) Cooks, R. G.; Ouyang, Z.; Takats, Z.; Wiseman, J. M. *Science* **2006**, *311*, 1566−1570.
(11) Harris, G. A.; Galhena, A. S.; Fernández, F. M. *Anal. Chem.* **2011**, *83*, 4508−4538.
(12) Monge, M. E.; Harris, G. A.; Dwivedi, P.; Fernández, F. M. *Chem. Rev.* **2013**, *113*, 2269−2308.
(13) Perry, R. H.; Splendore, M.; Chien, A.; Davis, N. K.; Zare, R. N. *Angew. Chem., Int. Ed.* **2011**, *50*, 250−254.
(14) Perry, R. H.; Brownell, K. R.; Chingin, K.; Cahill, T. J.; Waymouth, R. M.; Zare, R. N. *Proc. Natl. Acad. Sci. U. S. A.* **2012**, *109*, 2246−2250.
(15) Perry, R. H.; Cahill, T. J.; Roizen, J. L.; Du Bois, J.; Zare, R. N. *Proc. Natl. Acad. Sci. U. S. A.* **2012**, *109*, 18295−18299.
(16) Takáts, Z.; Wiseman, J. M.; Gologan, B.; Cooks, R. G. *Anal. Chem.* **2004**, *76*, 4050−4058.
(17) Wang, R.; Allmendinger, P.; Zhu, L.; Gröhn, A. J.; Wegner, K.; Frankevich, V.; Zenobi, R. *J. Am. Soc. Mass Spectrom.* **2011**, *22*, 1234−41.
(18) Wolk, A. B.; Leavitt, C. M.; Garand, E.; Johnson, M. A. *Acc. Chem. Res.* **2013**, in press, DOI: 10.1021/ar400125a.
(19) Wolk, A. B.; Leavitt, C. M.; Fournier, J. A.; Kamrath, M. Z.; Wijeratne, G. B.; Jackson, T. A.; Johnson, M. A. *Int. J. Mass Spectrom.* **2013**, in press, DOI: 10.1016/j.ijms.2013.04.022.
(20) Blakemore, J. D.; Schley, N. D.; Balcells, D.; Hull, J. F.; Olack, G. W.; Incarvito, C. D.; Eisenstein, O.; Brudvig, G. W.; Crabtree, R. H. *J. Am. Chem. Soc.* **2010**, *132*, 16017−16029.
(21) Zhou, M.; Schley, N. D.; Crabtree, R. H. *J. Am. Chem. Soc.* **2010**, *132*, 12550−12551.
(22) Parent, A. R.; Brewster, T. P.; De Wolf, W.; Crabtree, R. H.; Brudvig, G. W. *Inorg. Chem.* **2012**, *51*, 6147−6152.
(23) Zhou, M.; Hintermair, U.; Hashiguchi, B. G.; Parent, A. R.; Hashmi, S. M.; Elimelech, M.; Periana, R. A.; Brudvig, G. W.; Crabtree, R. H. *Organometallics* **2013**, *32*, 957−965.
(24) Savini, A.; Belanzoni, P.; Bellachioma, G.; Zuccaccia, C.; Zuccaccia, D.; Macchioni, A. *Green Chem.* **2011**, *13*, 3360.
(25) Grotjahn, D. B.; Brown, D. B.; Martin, J. K.; Marelius, D. C.; Abadjian, M.-C.; Tran, H. N.; Kalyuzhny, G.; Vecchio, K. S.; Specht, Z. G.; Cortes-Llamas, S. A.; Miranda-Soto, V.; van Niekerk, C.; Moore, C. E.; Rheingold, A. L. *J. Am. Chem. Soc.* **2011**, *133*, 19024−19027.
(26) Hintermair, U.; Hashmi, S. M.; Elimelech, M.; Crabtree, R. H. *J. Am. Chem. Soc.* **2012**, *134*, 9785−9795.
(27) Hintermair, U.; Sheehan, S. W.; Parent, A. R.; Ess, D. H.; Richens, D. T.; Vaccaro, P. H.; Brudvig, G. W.; Crabtree, R. H. *J. Am. Chem. Soc.* **2013**, *135*, 10837−10851.
(28) Perry, R. H.; Cooks, R. G.; Noll, R. J. *Mass Spectrom. Rev.* **2008**, *27*, 661−699.
(29) Santos, L. S.; Metzger, J. O. *Angew. Chem., Int. Ed.* **2006**, *45*, 977−981.
(30) Kamrath, M. Z.; Relph, R. A.; Guasco, T. L.; Leavitt, C. M.; Johnson, M. A. *Int. J. Mass Spectrom.* **2011**, *300*, 91−98.
(31) Kamrath, M. Z.; Garand, E.; Jordan, P. A.; Leavitt, C. M.; Wolk, A. B.; Van Stipdonk, M. J.; Miller, S. J.; Johnson, M. A. *J. Am. Chem. Soc.* **2011**, *133*, 6440−6448.
(32) Leavitt, C. M.; Wolk, A. B.; Fournier, J. A.; Kamrath, M. Z.; Garand, E.; Van Stipdonk, M. J.; Johnson, M. A. *J. Phys. Chem. Lett.* **2012**, *3*, 1099.
(33) Elliott, B. M.; Relph, R. A.; Roscioli, J. R.; Bopp, J. C.; Gardenier, G. H.; Guasco, T. L.; Johnson, M. A. *J. Chem. Phys.* **2008**, *129*, 094303.
(34) Frisch, M. J.; Trucks, G. W.; Schlegel, H. B.; Scuseria, G. E.; Robb, M. A.; Cheeseman, J. R.; Scalmani, G.; Barone, V.; Mennucci,

B.; Petersson, G. A.; Nakatsuji, H.; Caricato, M.; Li, X.; Hratchian, H. P.; Izmaylov, A. F.; Bloino, J.; Zheng, G.; Sonnenberg, J. L.; Hada, M.; Ehara, M.; Toyota, K.; Fukuda, R.; Hasegawa, J.; Ishida, M.; Nakajima, T.; Honda, Y.; Kitao, O.; Nakai, H.; Vreven, T.; Montgomery, Jr., J. A.; Peralta, J. E.; Ogliaro, F.; Bearpark, M.; Heyd, J. J.; Brothers, E.; Kudin, K. N.; Staroverov, V. N.; Kobayashi, R.; Normand, J.; Raghavachari, K.; Rendell, A.; Burant, J. C.; Iyengar, S. S.; Tomasi, J.; Cossi, M.; Rega, N.; Millam, J. M.; Klene, M.; Knox, J. E.; Cross, J. B.; Bakken, V.; Adamo, C.; Jaramillo, J.; Gomperts, R.; Stratmann, R. E.; Yazyev, O.; Austin, A. J.; Cammi, R.; Pomelli, C.; Ochterski, J. W.; Martin, R. L.; Morokuma, K.; Zakrzewski, V. G.; Voth, G. A.; Salvador, P.; Dannenberg, J. J.; Dapprich, S.; Daniels, A. D.; Farkas, Ö.; Foresman, J. B.; Ortiz, J. V.; Cioslowski, J.; Fox, D. J. *Gaussian 09*, Revision A.02; Gaussian, Inc.: Wallingford, CT, 2009.

(35) Yanai, T.; Tew, D. P.; Handy, N. C. *Chem. Phys. Lett.* **2004**, *393*, 51−57.

(36) Garand, E.; Fournier, J. A.; Kamrath, M. Z.; Schley, N. D.; Crabtree, R. H.; Johnson, M. A. *Phys. Chem. Chem. Phys.* **2012**, *14*, 10109−13.

(37) Van Berkel, G.; Kertesz, V. *Anal. Chem.* **2007**, *79*, 5510−5520.

(38) Pasilis, S. P.; Kertesz, V.; Van Berkel, G. J. *Anal. Chem.* **2008**, *80*, 1208−1214.

(39) Benassi, M.; Wu, C.; Nefliu, M.; Ifa, D. R.; Volný, M.; Cooks, R. G. *Int. J. Mass Spectrom.* **2009**, *280*, 235−240.

(40) Schley, N. D.; Halbert, S.; Raynaud, C.; Eisenstein, O.; Crabtree, R. H. *Inorg. Chem.* **2012**, *51*, 12313−12323.

(41) Girod, M.; Moyano, E.; Campbell, D. I.; Cooks, R. G. *Chem. Sci.* **2011**, *2*, 501.

(42) Müller, T.; Badu-Tawiah, A.; Cooks, R. G. *Angew. Chem., Int. Ed.* **2012**, *51*, 11832−11835.

(43) Kebarle, P.; Tang, L. *Anal. Chem.* **1993**, *65*, 972A−986A.

(44) Peschke, M.; Verkerk, U. H.; Kebarle, P. *J. Am. Soc. Mass Spectrom.* **2004**, *15*, 1424−1434.

(45) Kebarle, P.; Verkerk, U. *React. Intermed.* **2010**, 1−35.

(46) Zhou, M.; Balcells, D.; Parent, A. R.; Crabtree, R. H.; Eisenstein, O. *ACS Catal.* **2012**, *2*, 208−218.

(47) Zuccaccia, C.; Bellachioma, G.; Bolaño, S.; Rocchigiani, L.; Savini, A.; Macchioni, A. *Eur. J. Inorg. Chem.* **2012**, *2012*, 1462−1468.

(48) Robertson, W. H.; Karapetian, K.; Ayotte, P.; Jordan, K. D.; Johnson, M. A. *J. Chem. Phys.* **2002**, *116*, 4853.

(49) It is unclear why the oxidation of **2(OH)** is more extensive at lower concentrations and on PTFE surfaces. Identical studies using dilute solutions of **1(OH)** on PTFE showed more extensive oxidation of **1(OH)** than depositing the more concentrated solutions on paper, suggesting that these conditions in general access greater evident conversion of deposited species to oxidized product.